AIP Applied Physics Letters

Suppression of thermal conductivity in InxGa1−xN alloys by nanometer-scale disorder

T. Tong, D. Fu, A. X. Levander, W. J. Schaff, B. N. Pantha et al.

Citation: Appl. Phys. Lett. 102, 121906 (2013); doi: 10.1063/1.4798838
View online: http://dx.doi.org/10.1063/1.4798838
View Table of Contents: http://apl.aip.org/resource/1/APPLAB/v102/i12
Published by the American Institute of Physics.

Related Articles

Simultaneous measurement of thermal conductivity and heat capacity of bulk and thin film materials using frequency-dependent transient thermoreflectance method
Rev. Sci. Instrum. 84, 034902 (2013)

Onset of size effect in lattice thermal conductivity of thin films
J. Appl. Phys. 113, 113511 (2013)

Effects of valence-band mixing and strain on thermoelectric properties of p-type quantum wells
J. Appl. Phys. 113, 113706 (2013)

Equilibrium molecular dynamics simulations for the thermal conductivity of Si/Ge nanocomposites
J. Appl. Phys. 113, 104306 (2013)

Thermoelectric properties of intermetallic semiconducting RuIn3 and metallic IrIn3
J. Appl. Phys. 113, 083709 (2013)

Additional information on Appl. Phys. Lett.

Journal Homepage: http://apl.aip.org/
Journal Information: http://apl.aip.org/about/about_the_journal
Top downloads: http://apl.aip.org/features/most_downloaded
Information for Authors: http://apl.aip.org/authors

ADVERTISEMENT

AIP Applied Physics Letters
EXPLORE WHAT'S NEW IN APL
SUBMIT YOUR PAPER NOW!
SURFACES AND INTERFACES
Focusing on physical, chemical, biological, structural, optical, magnetic and electrical properties of surfaces and interfaces, and more...
ENERGY CONVERSION AND STORAGE
Focusing on all aspects of static and dynamic energy conversion, energy storage, photovoltaics, solar fuels, batteries, capacitors, thermoelectrics, and more...

Downloaded 27 Mar 2013 to 129.118.19.187. This article is copyrighted as indicated in the abstract. Reuse of AIP content is subject to the terms at: http://apl.aip.org/about/rights_and_permissions

Suppression of thermal conductivity in $In_xGa_{1-x}N$ alloys by nanometer-scale disorder

T. Tong,[1,a)] D. Fu,[2,3] A. X. Levander,[2,4] W. J. Schaff,[5] B. N. Pantha,[6] N. Lu,[7] B. Liu,[3] I. Ferguson,[7] R. Zhang,[3] J. Y. Lin,[6] H. X. Jiang,[6] J. Wu,[2,4] and David G. Cahill[1]
[1]Department of Materials Science and Engineering and Materials Research Laboratory, University of Illinois Urbana, Illinois 61801, USA
[2]Department of Materials Science and Engineering, University of California, Berkeley, California 94720, USA
[3]Jiangsu Provincial Key Laboratory of Advanced Photonic and Electronic Materials, School of Electronic Science and Engineering, Nanjing University, Nanjing, Jiangsu 210093, People's Republic of China
[4]Materials Sciences Division, Lawrence Berkeley National Laboratory, Berkeley, California 94720, USA
[5]Department of Electrical and Computer Engineering, Cornell University, Ithaca, New York 14853, USA
[6]Department of Electrical and Computer Engineering, Texas Tech University, Lubbock, Texas 79409, USA
[7]Department of Electrical and Computer Engineering, University of North Carolina, Charlotte, North Carolina 28223, USA

(Received 9 October 2012; accepted 18 March 2013; published online 27 March 2013)

We have systematically measured the room-temperature thermal conductivity of epitaxial layers of $In_xGa_{1-x}N$ alloys with 15 different Indium compositions ranging from 0.08 to 0.98 by time-domain thermoreflectance method. The data are compared to the estimates of the strength of phonon scattering by cation disorder. The thermal conductivity is in good agreement with the theoretical modeling results based on the mass difference for In-rich ($x > 0.9$) and Ga-rich ($x < 0.2$) compositions. At intermediate compositions ($0.2 < x < 0.9$), the thermal conductivity is strongly suppressed below the values expected for homogeneous alloys. We attribute this suppression of thermal conductivity to phonon scattering by nanometer-scale compositional inhomogeneities in alloys. © *2013 American Institute of Physics*. [http://dx.doi.org/10.1063/1.4798838]

$In_xGa_{1-x}N$ alloys with Ga-rich compositions ($x < 0.3$) are used as active layers for light emitting diodes in the short-wavelength region, $400 < \lambda < 530$ nm. Applications at longer wavelengths, green emission, are limited by an abrupt drop in the quantum efficiency that typically occurs at $x > 0.3$.[1] Compositional inhomogeneities and structural defects have been proposed as possible reasons for this drop in quantum efficiency.[2] We have recently demonstrated that thermal conductivity measurements can reveal disorder in epitaxial layers that is difficult to identified by traditional x-ray diffraction (XRD) or transmission electron microscopy (TEM).[3] Here, we use thermal conductivity measurements to reveal nanometer-scale disorder in $In_xGa_{1-x}N$ alloys that extends over a wide range of compositions, and the results indicate the strongest disorder exists for compositions $0.2 < x < 0.6$, approximately corresponding to the $In_xGa_{1-x}N$ miscibility gap.[4,5]

$In_xGa_{1-x}N$ alloys show promise for efficient thermoelectric energy conversion in addition to their applications in solid-state lighting.[6,7] The thermoelectric figure-of-merit, $ZT = S^2\sigma T/\Lambda$, where S, σ, Λ, and T are the Seebeck coefficient, electrical conductivity, thermal conductivity, and temperature, respectively, has been reported to be comparable to the figure-of-merit of SiGe alloys.[6,8] High-efficiency conversion of heat into electrical power requires low lattice thermal conductivity while maintaining high mobility of the charge carriers. The binary InN and GaN materials have high thermal conductivity materials[9–14] (the room-temperature thermal conductivity of GaN and InN are 230 and 120 $W m^{-1} K^{-1}$, respectively); however, the thermal conductivity of even relatively dilute $In_xGa_{1-x}N$ alloys is significantly reduced because of scattering of high-frequency phonons by mass disorder.[15]

Four sets of $In_xGa_{1-x}N$ epitaxial layers with various thicknesses were grown by molecular beam epitaxy (MBE) and metalorganic chemical vapor deposition (MOCVD) on *c*-sapphire substrates at four different institutions.[16–18] Growth conditions, sample structures, compositions, and thermal conductivities are summarized in Table I. Sample numbers 5 and 9 were the subject of a prior study of composition modulation in $In_xGa_{1-x}N$ alloys by TEM and XRD.[17] Liliental-Weber *et al.* (see Ref. 16) observed periodic modulations in composition along the *c*-axis with a period of ≈5 nm for $x = 0.55$ and ≈7 nm for $x = 0.78$. They observed a columnar growth morphology with columns separated by edge dislocations, where the average dislocation density was $\approx 10^{11}$ cm^{-2} and 6×10^{10} cm^{-2} for $x = 0.55$ and $x = 0.78$, respectively.

Figure 1(a) shows XRD θ-2θ scan data of the (0002) reflections for selected $In_xGa_{1-x}N$ samples. All samples show a single (0002) reflection; the lack of secondary peaks indicates that these samples do not exhibit gross extended domains that are phase-separated into Ga-rich and In-rich alloys.[19,20] Figure 1(b) shows the $In_xGa_{1-x}N$ *c*-lattice parameter as a function of the In content of selected samples determined by Rutherford backscattering spectrometry (RBS). The *c*-lattice parameters are in good agreement with Vegard's law, where the layers are assumed to be fully relaxed. The full-width-at-half-maximum (FWHM) of the XRD peaks is plotted in Fig. 1(c). The XRD peaks are strongly broadened, presumably by inhomogeneous strain fields created by plastic deformation that relaxes the epitaxial stresses imposed by the substrate.

a)Author to whom correspondence should be addressed. Electronic mail: tong16@illinois.edu

0003-6951/2013/102(12)/121906/5/$30.00

© 2013 American Institute of Physics

Downloaded 27 Mar 2013 to 129.118.19.187. This article is copyrighted as indicated in the abstract. Reuse of AIP content is subject to the terms at: http://apl.aip.org/about/rights_and_permissions

TABLE I. Summary of all $In_xGa_{1-x}N$ samples investigated. The samples were grown by MOCVD or MBE method on sapphire substrates with GaN or AlN buffer layers at four institutions. The composition is determined by XRD and RBS. The thermal conductivities are measured by time-domain thermoreflectance.

Samples	Growth technique	In fraction (RBS)	In fraction (XRD)	Thickness (nm)	Buffer layer	Thermal conductivity Λ(W m^{-1} K^{-1})
1	MOCVD	0.08	0.07	229	GaN	24
2	MOCVD	0.11	0.10	233	GaN	13
3	MOCVD	0.17	0.16	268	GaN	8.5
4	MOCVD	0.25	0.25	608	AlN	2.8
5	MBE	0.44	0.48	147	GaN	2.2
6	MBE	0.56	0.55	398	GaN	2.5
7	MOCVD	0.64	0.65	560	AlN	3.8
8	MBE	0.70	0.64	500	GaN	4.1
9	MBE	0.72	0.72	364	GaN	4.3
10	MBE	0.80	0.78	302	None	5.1
11	MOCVD	0.80	0.82	723	AlN	5.3
12	MOCVD	0.79	0.83	223	GaN	4.8
13	MOCVD	0.84	0.90	222	GaN	5.6
14	MOCVD	0.90	0.93	756	AlN	8.5
15	MBE	0.98	0.99	4600	GaN	73

Each sample was coated with a $\approx$80 nm thick layer of Al by magnetron sputter deposition at room temperature to prepare the samples for thermal conductivity measurements. This Al layer serves as an optical transducer in the measurement of thermal conductivity by time-domain thermoreflectance (TDTR).[21] Details of the measurement setup are described in Ref. 22. In a TDTR measurement, a laser beam from a mode-locked Ti: sapphire laser is split into a pump beam and a probe beam with the relative optical path adjusted by a mechanical delay stage. The pump beam is modulated at 9.8 MHz by an electro-optic modulator. The pump and probe beam are focused on the sample to a $1/e^2$ radius of $\approx 5\,\mu$m. The Al layer is heated by the pump beam, and the temperature change of the Al layer is monitored by the probe beam through the temperature dependence of the optical reflectivity of Al. Signals obtained by a photodetector are sent to a lock-in amplifier to detect the 9.8 MHz component that is synchronous with the modulation of the pump beam.

The ratio of in-phase (V_{in}) and out-of-phase (V_{out}) signals were compared with a multilayer thermal transport model.[21] Fitting parameters used in the model include thickness, heat capacity, and thermal conductivity of each layer. The Al thickness was determined by picosecond acoustics. The rule of mixtures was used to calculate heat capacities of $In_xGa_{1-x}N$ alloys, $C_{InGaN} = xC_{InN} + (1-x)C_{GaN}$; here $C_{InN} = 2.1$ J cm^{-3} K^{-1} (Ref. 23) and $C_{GaN} = 2.6$ J cm^{-3} K^{-1}.[24] The thermal penetration depth is $\delta = \sqrt{\Lambda/(C\pi f)} \approx 200$nm. Alloy layers with thickness $d > \delta$ are "thermally thick," and the thermal conductance of the alloy-layer/buffer-layer interface G_b and the thermal conductivity of buffer-layer are unimportant in the model. Since the acoustic impedance difference between alloy layers and GaN buffer layers is small, for the low-In alloy layers with $d < \delta$, it can expected that the interfacial thermal conductance is high. Furthermore, the intermediate In composition alloys with $d < \delta$ grown on high thermal conductivity GaN buffer layers produce only a small correction to the model. Hence, we do not include the interfacial thermal conductance in the model. Since the samples grown on AlN buffer layers are thermally thick, the uncertainty of the thermal conductivity of AlN layers which could be as low as 1 W m^{-1} K^{-1} (Ref. 25) has no effect on the model. The thermal conductivity of the $In_xGa_{1-x}N$ layer and the thermal conductance of the interface between the Al layer and the $In_xGa_{1-x}N$ layer are the only significant unknowns. These two free parameters were adjusted to give the best fit between the model and the experimental data.

The thermal conductivity of $In_xGa_{1-x}N$ alloys at room temperature is plotted in Fig. 2(a). We include data from prior studies of $In_xGa_{1-x}N$ alloys for comparison. Sztein *et al.* studied *n*-type $In_xGa_{1-x}N$ films (81–190 nm thick) deposited by MOCVD[26] on Fe:GaN/sapphire. Pantha *et al.* studied $In_xGa_{1-x}N$ films ($\approx$110 nm thick) grown by MOCVD on GaN/sapphire templates. In these studies, the thermal conductivity of the epitaxial layers was measured by a differential 3ω method. The thermal conductivity of $In_xGa_{1-x}N$ alloys reaches a minimum in our dataset of 2.2 W m^{-1} K^{-1} at $x = 0.44$.

A Callaway model[27] as modified by Morreli *et al.*[28] is used to calculate the lattice thermal conductivity to gain quantitative insight into the strength of the phonon scattering mechanisms. In this model, the longitudinal and transverse phonon modes are independently investigated. The total thermal conductivity is a sum over one longitudinal (Λ_L) and two degenerate transverse (Λ_T) components, $\Lambda = \Lambda_L + 2\Lambda_T$, where $\Lambda_L = \Lambda_{L1} + \Lambda_{L2}$ and $\Lambda_T = \Lambda_{T1} + \Lambda_{T2}$. The partial conductivities Λ_{L1}, Λ_{L2}, Λ_{T1}, and Λ_{T2} are the Debye-Callaway terms (see Eqs. (3a), (3b), (4a), and (4b) of Ref. 28). Debye temperatures and speeds of sound are calculated separately for acoustic phonon branches in the [001] direction. The cut-off frequencies f_c are set at the zone boundary of the acoustic phonon dispersion curves, and the Debye temperatures were calculated from these frequencies, $T_D = hf_c/k_B$, where k_B is Boltzmann constant.

Grüneisen parameters of $\gamma_L = 0.73$ and $\gamma_T = 0.51$ were assumed for all alloy compositions,[29] and a virtual crystal model was used to determine the speeds of sound, densities, and cut-off frequencies of the alloys. The longitudinal speeds

Downloaded 27 Mar 2013 to 129.118.19.187. This article is copyrighted as indicated in the abstract. Reuse of AIP content is subject to the terms at: http://apl.aip.org/about/rights_and_permissions

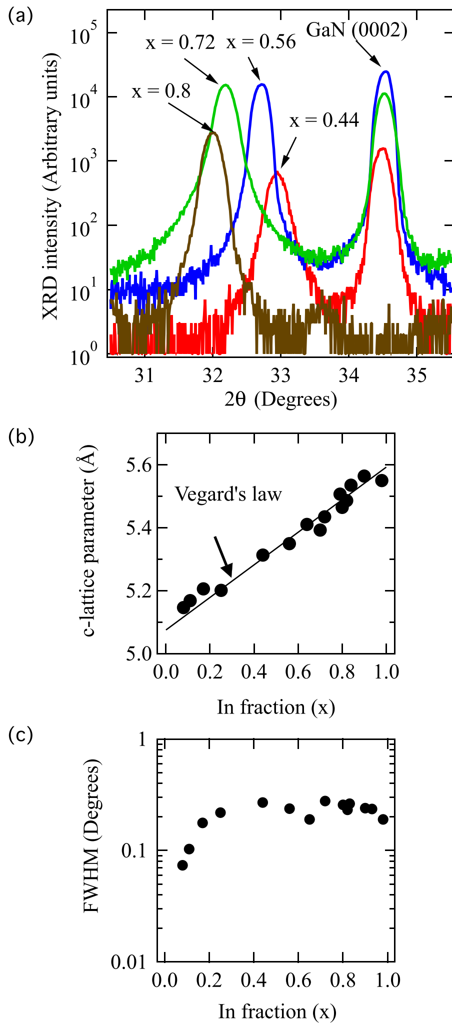

FIG. 1. (a) XRD θ-2θ scan patterns for selected $In_xGa_{1-x}N$ samples in the vicinity of the (0002) reflection. (b) XRD c-lattice parameter of $In_xGa_{1-x}N$ alloys vs. In composition measured by RBS. The solid line shows the prediction of Vegard's law; the good agreement suggests that the $In_xGa_{1-x}N$ layers are fully relaxed. (c) FWHM of the $In_xGa_{1-x}N$ (0002) reflection vs. In composition.

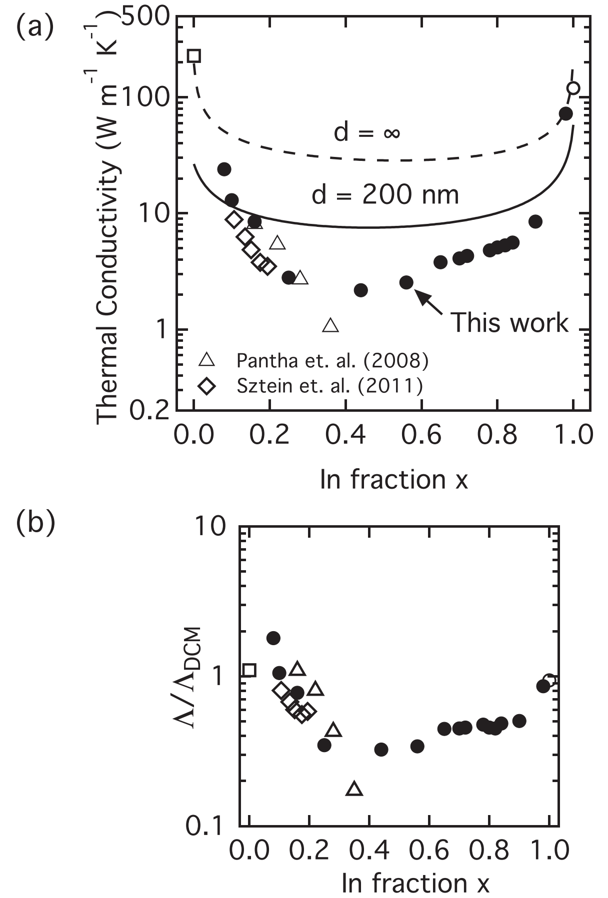

FIG. 2. (a) The thermal conductivity (Λ) at room temperature of $In_xGa_{1-x}N$ alloys as a function of In fraction compared to the predictions of the modified Callaway model. Previously reported thermal conductivities of GaN, InN, and $In_xGa_{1-x}N$ alloys are included for comparison. The open-square and open-circle is the thermal conductivity of pure GaN (Ref. 9) and pure InN (Ref. 10), respectively. The dashed line is calculated for the limit of large layer thickness; the solid line is calculation for a layer thickness of $d = 200$ nm. (b) Ratio of the measured thermal conductivity from this work to the calculated thermal conductivity (Λ_{DCM}) at each thickness as a function of In content.

of sound were measured for selected samples ($x = 0.44$, 0.65, 0.9, and 0.93) by picosecond acoustics to provide greater confidence in the validity of this approximation. The data are in good agreement with the virtual crystal approximation. Table II summarizes the parameters used in our model.

The resistive scattering rate includes contributions from phonon-phonon Umklapp scattering (τ_U), point defect scattering due to mass disorder and bond length disorder (τ_I), and boundary scattering (τ_B). Typically the high temperature form of the normal process scattering rate[32] is taken as[33]

$$(\tau_N)^{-1} = \frac{k_B \gamma^2 V^{1/3}}{M v^3} \omega^2 T. \qquad (1)$$

Here, γ is the Grüneisen parameter, V is the volume per atom, M is the average mass of the atoms in the alloys given by $M = xM_A + (1-x)M_B$ and M_A, M_B are the atomic weights of alloy components (GaN and InN for $In_xGa_{1-x}N$ alloys), v is speed of sound, and ω is the phonon frequency.

Klemens derived a form of the phonon scattering due to point defect disorder[34]

$$(\tau_I)^{-1} = \frac{\Gamma V}{4\pi v^3} \omega^4. \qquad (2)$$

Γ is a coefficient that characterizes the strength of phonon scattering and for mass disorder in alloys with a basis of 2 atoms[35]

$$\Gamma = x\left(\frac{M_A - M}{M}\right)^2 + (1-x)\left(\frac{M_B - M}{M}\right)^2. \qquad (3)$$

The phonon boundary scattering rate is given by $(\tau_B)^{-1} = v/d$, where d is the thickness of the sample and v

TABLE II. Material parameters of InN and GaN used in the Callaway-type model of the thermal conductivity of $In_xGa_{1-x}N$ alloys.

	T_D^L [a] (K)	T_D^L [a] (K)	v_L [b] (m/s)	v_T [b] (m/s)
InN	278	194	5720	2650
GaN	305	157	7770	3950

[a] T_D^L and T_D^T are, respectively, longitudinal and transverse cut-off Debye temperatures calculated from Ref. 30.
[b] v_L and v_T are, respectively, speeds of sound for longitudinal and transverse phonon dispersion branches calculated from Ref. 31.

Downloaded 27 Mar 2013 to 129.118.19.187. This article is copyrighted as indicated in the abstract. Reuse of AIP content is subject to the terms at: http://apl.aip.org/about/rights_and_permissions

velocity of each acoustic mode. The thicknesses of the samples in our study are not constant, but the dependence of the model on the boundary scattering rate is weak (changing d by a factor of 2 creates a change in the thermal conductivity of a factor of 1.2). Moreover, since the thermal conductivity of semiconductor alloys measured by TDTR is not governed by the phonons with mean free paths larger than the thermal penetration depth,[36] the thermal penetration depth can be used as an effective film thickness for alloys with $d > \delta$.

The contribution of phonon scattering by dislocation cores and the long-ranged strain field of dislocations was also considered.[37] Dislocations significantly reduce the thermal conductivity of high thermal conductivity pure crystals such as GaN.[25] However, these calculations show that the disorder alloy scattering rate is approximately an order of magnitude higher than the dislocation scattering rate even for a very high dislocation density of $10^{12}\,cm^{-2}$. Inclusion of the dislocation scattering rate at a density of $10^{12}\,cm^{-2}$ suppresses the thermal conductivity by only $\approx$10% for In compositions $0.2 < x < 0.9$. Therefore, phonon scattering by dislocations was not used in this model.

The solid line in the Fig. 2(a) shows the results of this calculation for the thermal conductivity as a function of InN composition at a fixed thickness of 200 nm, which is the average value of the effective thickness of the films. It is noted that the calculated thermal conductivity of the pure GaN and InN samples is much smaller than the experimental data. This discrepancy is created by the boundary scattering in this model, which creates a much stronger reduction of the thermal conductivity of the pure crystals than the alloy (the thicknesses of the GaN and InN layers were 200 μm and 1 μm, respectively). If the boundary scattering is removed, this model (the dashed line in the Fig. 2(a)) matches the experimental values of pure InN and GaN. The thermal conductivity at each thickness is also calculated and plotted as the ratio of the measured thermal conductivity and the calculated thermal conductivity as a function of In composition in Fig. 2(b). It is noted that the thermal conductivity of the alloy layer with $x = 0.08$ is higher than calculation by the model. One possibility is that the boundary scattering is not as high as prediction because of small acoustic impedance mismatch between the alloy layer and the GaN buffer layer.

A significant reduction of the $In_xGa_{1-x}N$ thermal conductivity below the prediction of the model is observed for In compositions in the range $0.2 < x < 0.9$. This suppression is stronger for $0.2 < x < 0.6$ which falls within the miscibility gap. This reduction is much larger than the uncertainties in the TDTR experiment of $\pm$10% (the error bar is approximately the size of symbols used to plot the data points in Fig. 2(a)). While the model predicts well the thermal conductivity for the alloy with $x = 0.98$, the abrupt reduction of the thermal conductivity for $x < 0.9$ prevents using the possibility of bond-length disorder as a significant phonon-scattering mechanism in these alloys. Therefore the enhanced phonon scattering at $0.2 < x < 0.9$ is tentatively attributed to nanometer-scale compositional inhomogeneities in alloys that are thermodynamically unstable.[4,5] There has been no systematic study of the thermal conductivity of thermodynamically unstable alloys prior to this work, but the strong reduction of thermal conductivity by the precipitation of nanometer scale second phase particles has been widely investigated.[38,39]

The existence of compositional inhomogeneities in $In_xGa_{1-x}N$ has been controversial,[40–42] partly because electron-beam damage during imaging by TEM can generate changes in composition, and some of the early studies misinterpreted these experimental artifacts as compositional inhomogeneities formed during epitaxial growth. Low In content alloys have been best studied, and most of these studies have concluded that for $x < 0.20$ in the form of thin layers lattice matched to GaN, the microscopic structure is best described as a random alloy.[43,44] The microstructure of higher concentration alloys and unstrained layers have been less studied.[5]

In conclusion, at low and high In concentrations ($x < 0.2$ and $x > 0.9$), the thermal conductivity of $In_xGa_{1-x}N$ is adequately described by a model based on phonon Rayleigh scattering of mass disorders. At intermediate compositions, a suppression in the thermal conductivity has been observed which has been attributed to nanometer-scale compositional inhomogeneities that strongly scatter thermal phonons.

This work was supported by Office of Naval Research (Grant No. N000141010525) through the Frederick Seitz Materials Research Laboratory MRL at the University of Illinois at Urbana Champaign. The XRD and RBS work at Berkeley was supported by the NSF (Grant No. ECCS-1101779). The InGaN epi-growth work at Texas Tech University is supported by NSF (Grant No. DMR-0906879). The InGaN MOCVD growth work and XRD from University of North Carolina at Charlotte were supported by Energy Production Infrastructure Center (EPIC).

[1] J. Wu, J. Appl. Phys. **106**, 011101 (2009).
[2] J. M. Phillips, M. E. Coltrin, M. H. Crawford, A. J. Fischer, M. R. Krames, R. Mueller-Mach, G. O. Mueller, Y. Ohno, L. E. S. Rohwer, J. A. Simmons, and J. Y. Tsao, Laser Photonics Rev. **1**(4), 307 (2007).
[3] D. W. Oh, J. Ravichandran, C. W. Liang, W. Siemons, B. Jalan, C. M. Brooks, M. Huijben, D. G. Schlom, S. Stemmer, L. W. Martin, A. Majumdar, R. Ramesh, and D. G. Cahill, Appl. Phys. Lett. **98**(22), 221904 (2011).
[4] I. Ho and G. Stringfellow, Appl. Phys. Lett. **69**(18), 2701 (1996).
[5] G. B. Stringfellow, J. Cryst. Growth **312**(6), 735 (2010).
[6] B. N. Pantha, R. Dahal, J. Li, J. Y. Lin, H. X. Jiang, and G. Pomrenke, Appl. Phys. Lett. **92**, 042112 (2008).
[7] E. N. Hurwitz, M. Asghar, A. Melton, B. Kucukgok, L. Su, M. Orocz, M. Jamil, N. Lu, and I. T. Ferguson, J. Electron. Mater. **40**(5), 513 (2011).
[8] J. P. Dismukes, E. Ekstrom, D. S. Beers, E. F. Steigmeier, and I. Kudman, J. Appl. Phys. **35**(10), 2899 (1964).
[9] G. A. Slack, L. J. Schowalter, D. Morelli, and A. F. J. Jaime, J. Cryst. Growth **246**, 287 (2002).
[10] A. X. Levander, T. Tong, K. M. Yu, J. Suh, D. Fu, R. Zhang, H. Lu, W. J. Schaff, O. Dubon, W. Walukiewicz, D. G. Cahill, and J. Wu, Appl. Phys. Lett. **98**, 012108 (2011).
[11] Y. K. Koh, Y. Cao, D. G. Cahill, and D. Jena, Adv. Funct. Mater. **19**, 610 (2009).
[12] D. I. Florescu, V. M. Asnin, F. H. Pollak, A. M. Jones, J. C. Ramer, M. J. Schurman, and I. Ferguson, Appl. Phys. Lett. **77**, 1464 (2000).
[13] V. Asnin, F. Pollak, J. Ramer, M. Schurman, and I. Ferguson, Appl. Phys. Lett. **75**, 1240 (1999).
[14] E. K. Sichel and J. I. Pankove, J. Phys. Chem. Solids **38**, 330 (1977).
[15] P. Carruthers, Rev. Mod. Phys. **33**, 92 (1961).
[16] B. Pantha, J. Li, J. Y. Lin, and H. X. Jiang, Appl. Phys. Lett. **93**, 182107 (2008).
[17] Z. Liliental-Weber, D. N. Zakharov, K. M. Yu, J. W. Ager III, W. Walukiewicz, E. E. Haller, H. Lu, and W. J. Schaff, J. Electron Microsc. **54**, 243 (2005).

Downloaded 27 Mar 2013 to 129.118.19.187. This article is copyrighted as indicated in the abstract. Reuse of AIP content is subject to the terms at: http://apl.aip.org/about/rights_and_permissions

[18]B. Liu, W. Luo, R. Zhang, Z. Zou, Z. Xie, Z. Li, D. Chen, X. Xiu, P. Han, and Y. Zheng, Phys. Status Solidi C **7**, 1817 (2010).
[19]B. N. Pantha, J. Li, J. Y. Lin, and H. X. Jiang, Appl. Phys. Lett. **96**, 232105 (2010).
[20]R. Singh, D. Doppalapudi, T. Moustakas, and L. Romano, Appl. Phys. Lett. **70**(9), 1089 (1997).
[21]D. Cahill, Rev. Sci. Instrum. **75**(12), 5119 (2004).
[22]K. Kang, Y. K. Koh, C. Chiritescu, X. Zheng, and D. G. Cahill, Rev. Sci. Instrum. **79**(11), 114901 (2008).
[23]S. Krukowski, A. Witek, J. Adamczyk, J. Jun, M. Bockowski, I. Grzegory, B. Lucznik, G. Nowak, M. Wroblewski, A. Presz, S. Gierlotka, S. Stelmach, B. Palosz, S. Porowski, and P. Zinn, J. Phys. Chem. Solids **59**(3), 289 (1998).
[24]J. Leitner, A. Strejc, D. Sedmidubsky, and K. Ruzicka, Thermochim. Acta **401**(2), 169 (2003).
[25]Z. Su, L. Huang, F. Liu, J. P. Freedman, L. M. Porter, R. F. Davis, and J. A. Malen, Appl. Phys. Lett. **100**(20), 201106 (2012).
[26]A. Sztein, H. Ohta, J. E. Bowers, S. P. Denbaars, and S. Nakamura, J. Appl. Phys. **110**(12), 123709 (2011).
[27]J. Callaway, Phys. Rev. **113**, 1046 (1959).
[28]D. T. Morelli, G. A. Slack, and J. P. Heremans, Phys. Rev. B **66**, 195304 (2002).
[29]Y. Koh, Ph.D. dissertation, University of Illinois Urbana, 2010.
[30]C. Bungaro, K. Rapcewicz, and J. Bernholc, Phys. Rev. B **61**, 6720 (2000).
[31]A. F. Wright, J. Appl. Phys. **82**(6), 2833 (1997).
[32]D. G. Cahill, F. Watanabe, A. Rockett, and C. B. Vining, Phys. Rev. B **71**, 235202 (2005).
[33]C. Herring, Phys. Rev. **95**, 954 (1954).
[34]P. G. Klemens, Proc. Phys. Soc., London, Sect. A **68**, 1113 (1955).
[35]B. Abeles, Phys. Rev. **131**, 1906 (1963).
[36]Y. Koh and D. Cahill, Phys. Rev. B **76**(7), 075207 (2007).
[37]J. Zou, D. Kotchetkov, D. Florescu, F. Pollak, and A. A. Balandin, J. Appl. Phys. **92**, 2534 (2002).
[38]N. Mingo, D. Hauser, N. Kobayashi, M. Plissonnier, and A. Shakouri, Nano Lett. **9**, 711 (2009).
[39]Y. K. Koh, S. L. Singer, W. Kim, J. M. O. Zide, H. Lu, D. G. Cahill, A. Majumdar, and A. C. Gossard, J. Appl. Phys. **105**(5), 054303 (2009).
[40]T. Smeeton, M. Kappers, J. Barnard, M. Vickers, and C. Humphreys, Appl. Phys. Lett. **83**(26), 5419 (2003).
[41]C. Kisielowski and T. P. Bartel, Appl. Phys. Lett. **91**(17), 176101 (2007).
[42]M. J. Galtrey, R. A. Oliver, M. J. Kappers, C. J. Humphreys, D. J. Stokes, P. H. Clifton, and A. Cerezo, Appl. Phys. Lett. **90**(6), 061903 (2007).
[43]T. Schulz, T. Remmele, T. Markurt, M. Korytov, and M. Albrecht, J. Appl. Phys. **112**, 033106 (2012).
[44]V. B. Oezdoel, C. T. Koch, and P. A. van Aken, J. Appl. Phys. **108**(5), 056103 (2010).

Downloaded 27 Mar 2013 to 129.118.19.187. This article is copyrighted as indicated in the abstract. Reuse of AIP content is subject to the terms at: http://apl.aip.org/about/rights_and_permissions